DOI: 10.13009/EUCASS2025-325
11TH EUROPEAN CONFERENCE FOR AERONAUTICS AND SPACE SCIENCES (EUCASS)

Perturbed relative trajectory design for on-orbit servicing to uncooperative targets in geostationary orbits

Pietro Costantini[⋆†] *and Gabriella Gaias*[⋆]
[⋆]*Politecnico di Milano, Aerospace Science and Technology Dept.*
Via La Masa 34, 20156, Milan, Italy
pietro.costantini@mail.polimi.it · gabriella.gaias@polimi.it
[†]Corresponding author

Abstract

This study focuses on the relative trajectory design for safe rendezvous with non-cooperative targets in the geostationary orbit, where on-orbit servicing is increasingly relevant. An empirical formulation, previously used for differential aerodynamic drag, leverages the filter properties of the Hill-Clohessy-Wiltshire equations to model differential solar radiation pressure. The so-obtained analytical model is compared with literature references and validated through a numerical propagator that handles the satellites' absolute orbits. The relative orbital elements' framework formalises the dependence on different release times from a Keplerian station-keeping condition. These theoretical findings, along with the eccentricity/inclination vector separation, support the enhanced passive safety concepts derived for bounded and high-drift trajectories and are applied to a realistic case-study far-range rendezvous.

1. Introduction

This study focuses on the relative trajectory design for safe Rendezvous (RV) with non-cooperative targets, ensuring robustness to failures and perturbations. The growing importance of On-Orbit Servicing (OOS) technologies is driving advancements in tools and methods to support sustainable space operations. Specifically, in Geostationary Earth Orbit (GEO), many OOS missions are conducted due to the presence of highly valuable assets. However, the standardised concept of uncooperative operations used in Low Earth Orbit (LEO) cannot be directly applied in GEO, due to different dominant natural accelerations, larger characteristic distances, and the need for coordination into the co-location slot, which all impact design and duration of the RV operations. The time-invariant nature of the linearised equations of motion is shown to provide a sharp-passband filter to the input of the Hill Clohessy Wiltshire (HCW) equations in Colombo.[1] A simple empirical acceleration formula is suggested to reduce the errors in the prediction of the Global Positioning System ephemerides. This feature is exploited in Gaias *et al.*[6] to model the effects of the differential aerodynamic drag on the relative motion in near-circular LEO. In addition to the Earth's oblateness perturbation on the relative secular dynamics, an empirical form for non-conservative perturbations is introduced, employing the previously justified harmonic expression. The Lyapunov transformation between the linearised equations in Cartesian and Relative Orbital Elements (ROE)s states is introduced to exploit the immediate geometrical understanding in the elements' space, as well as to derive the expression of the mean time variations of certain in-plane elements that convey the effect of the tangential only perturbation. In this work, the empirical model is applied to describe the effect of the solar radiation pressure, which is significant at higher altitudes, as in the geosynchronous scenario. The literature presents several formulations to model the differential Solar Radiation Pressure (SRP) effect. Spiridonova develops a relative motion model for satellite formations in GEO, involving both gravitational and non-gravitational forces: the J_2 gravitational disturbance, SRP and third body influence.[10] However, no explicit State Transition Matrix (STM) form is obtained, and the approximated expression is only valid for short time steps. Guffanti and D'Amico build a general methodology applicable to quasi-nonsingular and nonsingular ROEs where the secular and long-periodic effects due to perturbing functions are incorporated.[8] Accordingly, three plant matrices modelling geopotential zonal harmonics, third body gravity and SRP are obtained by augmenting the state with force model parameters and applying the first-order Taylor expansion to the time derivatives of the mean absolute orbital elements. The models have no limitations in eccentricity but show

DOI: 10.13009/EUCASS2025-325

singularity for zero inclination cases, which can be solved by using the reduced formulation which only models differential SRP. The relative eccentricity and relative inclination vector variations due to SRP and third body are addressed. The state derivatives for SRP are computed for the ballistic coefficients and the Sun ephemerides, but the analytical augmented form is retrieved by neglecting the orbit position contribution, which is dominated by the difference in ballistic coefficients of the satellites. For unknown ballistic properties of the target, a model-free expression is presented, and the unmodeled effects of the eclipses are considered by augmenting the state with a net semi-major axis variation. Although being general in term of central and perturbing bodies, this model comes with the complexity of needing averaged elements to remoce short term oscillations. Luo *et al.* study the relative motion subject to SRP and trajectory uncertainty.[9] The analytical solution of the two-point boundary value problem for a proximity scenario with a V-bar keeping point is presented. The SRP forcing term direction, assuming the same direction of the two spacecraft with respect to the Sun, is expressed in dependence on the Sun phase angle and the solar declination in GEO. The magnitude depends on the difference in ballistic coefficients. The shadow region around the equinoxes is neglected because it consists of 5% of an orbit period in those days. The HCW are integrated to obtain the general form of the particular solution to be added to the nominal non-homogeneous linear system. An optimisation model, constituted by a differential evolution algorithm, is then presented, exploiting the described solution to obtain passive safety for the target and the collocated satellites; the covariance of the relative state is used. Finally, Fehse studies the effect of different release times from a Keplerian position-keeping configuration, to analyse the dependence of the SRP direction on the date and time.[4] The discrepancy of the perturbed trajectory when compared to the ideal evolution amounts to hundreds of meters after just a single orbit. For this reason, the need for collision avoidance and closed-loop control capability is required. Luo *et al.*[9] and Fehse[4] are based on the Cartesian state and thus lack the immediate geometrical interpretation provided by ROEs (in Fehse,[4] no rule is derived to forecast the different perturbed trajectories obtained from different initial times). In this study, the derivation process from Gaias *et al.*[6] is extended to model the most significant relative disturbance in GEO, differential SRP. The analytical model obtained in this way is compared both theoretically and numerically with the literature and validated through numerical integration. The evolution of the relative state under the effect of the differential non-conservative perturbation in terms of ROEs is analysed to understand the dependence on departure time and to derive new safety concepts. For this latter purpose, both bounded and high-drift phases are considered, and finally, a RV in the GEO orbital regime is simulated employing realistic control schemes. The simplicity of the obtained STM matrix makes the model derived in this paper suitable for an on-board application, where the desired accuracy level can be obtained by properly updating the empirical coefficients, from the ground or the navigation sensors.

Concerning the structure of this paper, after the introduction, in Section 2 the integration of the general solution of the HCW equations when subjected to an empirical forcing term is shown, specialising the coefficients under the hypothesis of differential SRP as the dominant perturbation. The unified HCW-ROE framework[7] is used to obtain the ROE-based solution. In Section 3, the new formulation is compared with the aforementioned analytical models from the literature, both theoretically and numerically, and a numerical validation with an absolute-based numerical propagator assesses the range of validity of the hypotheses. Section 4 analyses the dependence on the departure time under the effect of differential SRP in the ROE space, to generalise the results presented in Fehse[4] using the relative Cartesian state. The geometrical insight provided by ROEs is the foundation of the passive safety concepts both for bounded and high-drift segments, which enhances the Eccentricity/Inclination (E/I) vector separation concept from D'Amico and Montenbruck[2] in the perturbed GEO region. The design of a far-range RV is exposed, using finite-number impulsive schemes from the literature, to show the effectiveness of the introduced concepts comparing different alternatives. Finally, Section 5 resumes the advantages and validity of the model, and how the passive safety concepts influence the RV design in GEO.

2. Methodology

The relative dynamics is described by the HCW linear time invariant system of Equation (1), which is derived under the hypothesis of small intersatellite separation, retaining only first order terms, and on a circular reference orbit. Here, the local orbital frame is assumed as the Radial Transversal Normal (RTN) frame of the chief, where the x direction corresponds to the position vector of the Chief, the z axis is in the direction of the specific angular momentum of the chief, and y completes the right-handed triad. It can be seen that the in-plane and out-of-plane components are decoupled, and all terms oscillate at the mean motion frequency.

DOI: 10.13009/EUCASS2025-325

$$\begin{cases} \delta\ddot{x} - 3n^2\delta x - 2n\delta\dot{y} = 0 \\ \delta\ddot{y} + 2n\delta\dot{x} = 0 \\ \delta\ddot{z} + n^2\delta z = 0 \end{cases} \tag{1}$$

Equation (2) reports another possible state representation: the adimensional nonsingular ROEs. This state is defined from the Keplerian nonsingular elements, with $e_x = e\cos\omega$, $e_y = e\sin\omega$, respectively x and y components of the eccentricity vector, $u = \omega + M$ is the mean argument of latitude, M is the mean anomaly, a the semimajor axis, ω the argument of perigee, Ω the right ascension of the ascending node, and i the inclination. This set provides a better geometrical insight of the relative trajectory and eases the derivation of safety concepts based on E/I vector separation.[2] Moreover, for formation reconfigurations, the energy optimal manoeuvre coincides with the shortest path variation depicted in the ROE space.

$$\delta\boldsymbol{\alpha} = \begin{bmatrix} \delta a \\ \delta\lambda \\ \delta e_x \\ \delta e_y \\ \delta i_x \\ \delta i_y \end{bmatrix} = \begin{bmatrix} \Delta a / a_{\text{chief}} \\ \Delta u + \Delta\Omega\cos i_{\text{chief}} \\ \Delta e_x \\ \Delta e_y \\ \Delta i \\ \Delta\Omega\sin i_{\text{chief}} \end{bmatrix} \tag{2}$$

In the close-range domain, a Lyapunov transformation is introduced in[7] to directly transform the osculating ROEs set into the Cartesian relative state (Equation (3)). Its inverse $\boldsymbol{T^{-1}}(t)$ is used to obtain the ROE-based model from the general solution of the perturbed HCW equations.

$$\boldsymbol{T}^{-1}(t) = \begin{bmatrix} 4 & 0 & 0 & 0 & \frac{2}{n} & 0 \\ 0 & 1 & 0 & -\frac{2}{n} & 0 & 0 \\ 3c & 0 & 0 & \frac{s}{n} & 2\frac{c}{n} & 0 \\ 3s & 0 & 0 & -\frac{c}{n} & 2\frac{s}{n} & 0 \\ 0 & 0 & s & 0 & 0 & \frac{c}{n} \\ 0 & 0 & -c & 0 & 0 & \frac{s}{n} \end{bmatrix} \tag{3}$$

where, to streamline the notation, $c = \cos nt$, $s = \sin nt$, and n is the mean motion of the reference orbit.

2.1 HCW equations with empirical forcing term

The input accelerations to the system of equations can always be decomposed into elementary sinusoidal waves that shape the frequency spectrum. Based on Colombo,[1] the Linear Time Invariant (LTI) system of the HCW equations reacts with a forced response which coincides with the sum of the responses to the input simple waves. This behaviour recalls a filter that smooths out the spectral components outside the bands. The perturbation, although originally complex, results in relatively simple acceleration errors. For this reason, the general solution is obtained for the HCW equations subject to a generic perturbation expressed with the following empirical form, which can be fed to the nominal equations to model a general non-conservative perturbation:

$$\mathbf{f}_{\text{gen}}(t) = \begin{bmatrix} A_{\text{R}}\cos nt + B_{\text{R}}\sin nt + C_{\text{R}} \\ A_{\text{T}}\cos nt + B_{\text{T}}\sin nt + C_{\text{T}} \\ A_{\text{N}}\cos nt + B_{\text{N}}\sin nt + C_{\text{N}} \end{bmatrix} \tag{4}$$

Where R, T, and N refer respectively to RTN directions of the co-moving frame centred on the chief satellite. The sub-matrixes of the particular solution expressed in the Cartesian state are reported in Equations (5) and (6):

DOI: 10.13009/EUCASS2025-325

$$\mathbf{\Phi}^{\mathbf{R}}_{\mathbf{r,f}}(t) = \frac{1}{2n^2}\begin{bmatrix} nts & s-ntc & 2d \\ 2(ntc-s) & -4d+2nts & 4(s-nt) \\ 0 & 0 & 0 \end{bmatrix},$$
$$\mathbf{\Phi}^{\mathbf{T}}_{\mathbf{r,f}}(t) = \frac{1}{2n^2}\begin{bmatrix} 2(s-ntc) & 4d-2nts & 4(nt-s) \\ \Phi_{2,1} & \Phi_{2,2} & \Phi_{2,3} \\ 0 & 0 & 0 \end{bmatrix}, \tag{5}$$
$$\mathbf{\Phi}^{\mathbf{N}}_{\mathbf{r,f}}(t) = \frac{1}{2n^2}\begin{bmatrix} 0 & 0 & 0 \\ 0 & 0 & 0 \\ nts & s-ntc & 2d \end{bmatrix}$$

$$\mathbf{\Phi}^{\mathbf{R}}_{\mathbf{v,f}}(t) = \frac{1}{2n}\begin{bmatrix} s+ntc & nts & 2s \\ -2nts & 2(ntc-s) & -4d \\ 0 & 0 & 0 \end{bmatrix},$$
$$\mathbf{\Phi}^{\mathbf{T}}_{\mathbf{v,f}}(t) = \frac{1}{2n}\begin{bmatrix} 2nts & 2(s-ntc) & 4d \\ 4ntc-2s & -6d+4nts & 8s-6nt \\ 0 & 0 & 0 \end{bmatrix}, \tag{6}$$
$$\mathbf{\Phi}^{\mathbf{N}}_{\mathbf{v,f}}(t) = \frac{1}{2n}\begin{bmatrix} 0 & 0 & 0 \\ 0 & 0 & 0 \\ s+ntc & nts & 2s \end{bmatrix}$$

Where the suffix r and v denote, respectively, the position and velocity components, while f denotes the forced solution. Again, to streamline the notation, $d = 1 - c$. Moreover $\Phi_{2,1} = -6d + 4nts$, $\Phi_{2,2} = 10(s - nt) + 4ntd$, and $\Phi_{2,3} = 8d - 3(nt)^2$. To derive a ROE-based model, the inverse of the Lyapunov transformation $\boldsymbol{T^{-1}}(t)$, can be used to explicitly express the evolution of the perturbed ROEs from the relative Cartesian state.[7] The ROE solution is of the form of Equation (7):

$$\mathbf{\Phi}^{\mathbf{f}}_{\mathbf{ROE}}(t) = \frac{1}{n^2}\begin{bmatrix} [\mathbf{\Phi}^{\mathbf{f}}_{\mathbf{ip}}(t)] & \mathbf{0_{4\times3}} \\ \mathbf{0_{2\times6}} & [\mathbf{\Phi}^{\mathbf{f}}_{\mathbf{oop}}(t)] \end{bmatrix} \tag{7}$$

where the in-plane and out-of-plane sub-blocks are provided in Equations (8) and (9).

$$\mathbf{\Phi}^{\mathbf{f}}_{\mathbf{ip}}(t) = \begin{bmatrix} 0 & 0 & 0 & 2s & 2d & 2nt \\ -2s & -2d & -nt & -3d & 3(s-nt) & -\frac{3}{2}(nt)^2 \\ \frac{s^2}{2} & \frac{nt-cs}{2} & d & (nt+cs) & s^2 & 2s \\ -\frac{nt+cs}{2} & -\frac{s^2}{2} & -s & s^2 & nt-cs & 2d \end{bmatrix} \tag{8}$$

$$\mathbf{\Phi}^{\mathbf{f}}_{\mathbf{oop}}(t) = \begin{bmatrix} (nt+cs)/2 & s^2/2 & s \\ s^2/2 & (nt-cs)/2 & d \end{bmatrix} \tag{9}$$

These terms, right multiplied by a column vector $\mathbf{p}$ containing the empirical parameters, must be added to the homogeneous solution, respectively in HCW or ROEs.

2.2 Empirical coefficients specified on the SRP in GEO

OOS missions are strategical in the GEO region, where differential SRP is the dominant perturbation considering a proximity scenario. For this reason, the proposed model is specified in the GEO region and its performance are assessed in this context.

The coefficients to describe this differential acceleration are obtained from the SRP absolute cannonball model, applied to the chief reference orbit. Typical approximations from the literature are introduced to obtain an empirical-type perturbation:

- The satellites are approximated to spheres with constant reflectivity and area-to-mass ratio, and the dependence on the attitude is neglected.
- For GEO orbits, eclipses only take place in short periods at midnight for around 23 days around the equinoxes.[9] In the worst case, which is on the day of the equinoxes, the maximum eclipse duration is 74 minutes, the 5% of an orbit. For this reason, their influence can be neglected now, and it is sufficient to consider the average result of this effect. The shadow function ν_{shadow} can be taken as always unitary.

DOI: 10.13009/EUCASS2025-325

- Since Sun-Earth distance is definitely larger than the inter-satellite separation, the resultant force is considered aligned to the Sun-satellite line that coincides with the Earth's position around the Sun at the desired time.
- The differential SRP coefficient is introduced, whose use is justified by the small distance between the satellites, characterising the quantities related to the deputy spacecraft with the subscript "d", the others refer to the chief. This coefficient is defined as (Equation (10)).

$$\delta S_0 = c_{\mathrm{r,d}} \frac{A_{\mathrm{r,d}}}{m_d} - c_{\mathrm{r}} \frac{A_{\mathrm{r}}}{m} \tag{10}$$

  Where c_{r} refers to the radiation pressure coefficient that is related to the reflectivity properties of the surface of the vehicles, and $\frac{A_{\mathrm{r}}}{m}$ refers to the area-to-mass ratio.

By introducing the momentum flux, at 1 AU, $\frac{S}{c} = 4.56 \cdot 10^{-6} N/m^2$ the differential SRP magnitude can be finally written as Equation (11):

$$\delta p_{\mathrm{SRP}} = \nu_{shadow} \frac{S}{c} \delta S_0 \tag{11}$$

The Earth-Sun unit vector is rotated from the geocentric ecliptic frame to the geocentric equatorial frame and finally to the frame attached to the chief. Its components thus depend on λ (solar apparent ecliptic longitude) and ϵ (obliquity of the ecliptic plane) and the Keplerian elements of the chief orbit (the RAAN Ω, the inclination i and the mean argument of latitude u, in this work assumed coincident with the argument of latitude (for a circular orbit mean anomaly M and true anomaly ν coincide and $u = \omega + \nu = \omega + M$, where ω is the argument of the perigee). The non-null empirical coefficients are obtained by re-organizing these quantities in constant terms and cosinusoidal terms depending on u as in Equation (12).

$$\begin{aligned}
A_{\mathrm{R}} &= \delta p_{\mathrm{SRP}}[s_\lambda c_\varepsilon s_\Omega + c_\lambda c_\Omega] \\
B_{\mathrm{R}} &= \delta p_{\mathrm{SRP}}[s_\lambda c_\varepsilon c_\Omega c_i - c_\lambda s_\Omega c_i + s_\lambda s_\varepsilon s_i] \\
A_{\mathrm{T}} &= \delta p_{\mathrm{SRP}}[s_\lambda c_\varepsilon c_\Omega c_i - c_\lambda s_\Omega c_i + s_\lambda s_\varepsilon s_i] \\
B_{\mathrm{T}} &= \delta p_{\mathrm{SRP}}[-s_\lambda c_\varepsilon s_\Omega - c_\lambda c_\Omega] \\
C_{\mathrm{N}} &= \delta p_{\mathrm{SRP}}[-s_\lambda c_\varepsilon c_\Omega s_i + c_\lambda s_\Omega s_i + s_\lambda s_\varepsilon c_i]
\end{aligned} \tag{12}$$

The notation $s_{(-)} = \sin(-)$ and $c_{(-)} = \cos(-)$ is used. Note that $A_T = B_R$ and $A_R = -B_T$. Moreover, the formulation can be extended to $u_0 \neq 0$ exploiting the sine and cosine sum expressions.

2.3 ROE-based model

The values of the coefficients can be reduced to the linear variation of ROEs, as done in Gaias *et al.*[6] The augmented state in the case of SRP is Equation (13):

$$a\delta\boldsymbol{\alpha}_{\text{d-SRP}} = \begin{bmatrix} a\delta\boldsymbol{\alpha} \\ a\delta\dot{e}_x \\ a\delta\dot{e}_y \\ z_{\mathrm{oop}} \end{bmatrix} \tag{13}$$

where $z_{\mathrm{oop}} = \frac{C_N}{n^2}$ represent the fixed shift on the normal axis and has the dimensions of $[m]$, while the other additional coefficients are Equation (14):

$$\begin{aligned}
a\delta\dot{e}_x &= \frac{1}{n^2}\left(\frac{3n}{2} B_R\right) \\
a\delta\dot{e}_y &= \frac{1}{n^2}\left(-\frac{3n}{2} A_R\right)
\end{aligned} \tag{14}$$

and have the dimension of m/s.

DOI: 10.13009/EUCASS2025-325

3. Model performance analyses

3.1 Comparison with other methodologies

The developed model is compared both theoretically and numerically with analogous literature frameworks. While results are mainly aligned, some differences in the procedure can be found.

- Luo *et al.*[9] adopts a different combination of angles to describe the Sun position: the Sun phase angle α and the solar declination β. It can be shown that these quantities correspond to the Ecliptic → Earth Centered Inertial (ECI) → RTN sequence of rotations. The following integration in HCW does not introduce any difference, and the solution is expressed in the Cartesian state.
- In Spiridonova[10] the integration is performed directly in the ECI frame and exploiting a short time step approximation. The integration of the ECI → RTN rotation, which involves time-dependent terms, is not formally performed.
- Guffanti and D'Amico[8] derive their STM by assuming that the difference in spacecraft ballistic coefficient dominates the orbit position difference. The resulting coefficients depend on the apparent ephemerides of the Sun, but when reducing them to a GEO application these coincide with the empirical ones. The STM expression is not obtained by a convolution integral but by approximating the parameters as constant along each short time step, similarly to what is done in Spiridonova.[10]

Figure 1 shows how the models behave similarly for a common RV duration of a few (e.g. 4-5) days, given the parameters of Table 1.

Chief Initial Keplerian Elements					
$a[km]$	$e[-]$	$i[^\circ]$	$\Omega[^\circ]$	ω[deg]	$M[^\circ]$
$4.2166.0085 \cdot 10^4$	$1.236 \cdot 10^{-4}$	$4.349 \cdot 10^{-2}$	270.7	160.0	148.5
Initial Relative Orbital Elements					
$a\delta a[m]$	$a\delta\lambda[m]$	$a\delta e_x[m]$	$a\delta e_y[m]$	$a\delta i_x[m]$	$a\delta i_y[m]$
-30.0	-3500.0	200.0	200.0	-100.0	-100.0
Mission Timing and Propagation					
Initial Date: 2024-10-06 18:27:00			**Propagation Duration (orbits):** 10		
Propagation Step: $60s$					
SRP Properties					
Chief			**Deputy**		
Area [m^2]	Mass [kg]	c_r	Area [m^2]	Mass [kg]	c_r
40	1000	1.2	40	1700	1.2

Table 1: Mission parameters to compare the literature models. The SRP properties and the initial configurations are taken from Spiridonova,[10] while the initial date is chosen arbitrarily.

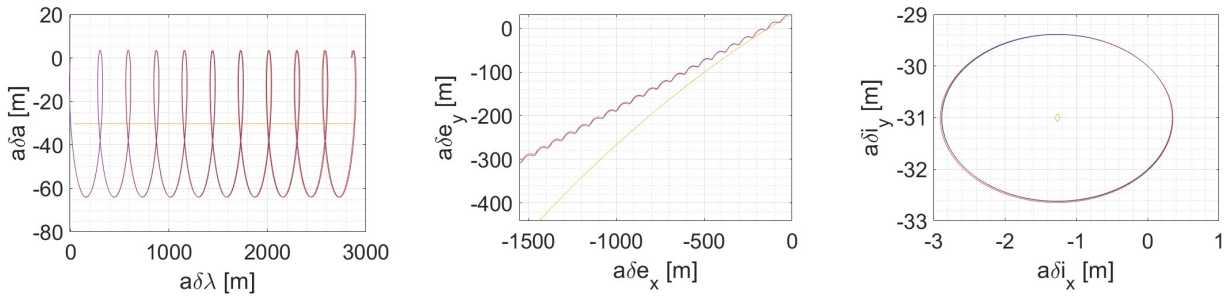

Figure 1: Respectively $a\delta\lambda/a\delta a$ and $a\delta e_x/a\delta e_y$ ROE planes describe the in-plane motion while $a\delta i_x/a\delta i_y$ describes the out-of-plane motion. The blue line represents the empirical formulation, while the models from the literature are shown in orange ([9]), purple ([10]), and yellow ([8]).

In the ROE framework, the model from Guffanti and D'Amico[8] is separated from the others. This is due to its nature, which captures the elements' mean evolution. An oscillatory motion is obtained for the

DOI: 10.13009/EUCASS2025-325

Cartesian state by applying the Lyapunov transform directly on the mean ROEs, hence without applying a mean-to-osculating transformation of the orbital elements. In this space, all models almost overlap, since the contribution of the short-periodic oscillations - neglected in Guffanti and D'Amico's model - is negligible compared to the overall variations in position and velocity over an orbit. Moreover, regarding the relative eccentricity motion, this last model diverges from the others since it is the only one describing the yearly circulation of the relative eccentricity vector and thus the most appropriate to describe the long-term trend of the elements. Concerning the other formulations, and specifically the empirical one derived in this work, the secular behaviour is captured as a linear drift of the relative eccentricity components but does not follow the yearly circulation when the parameters fed to the model are not updated. Instead, the overall evolution, incorporating long-periodic effects (the yearly circulation due to the apparent motion of the Sun around the Earth), can be recovered by updating the empirical coefficients at a sufficient frequency (the linear approximation works for a few days, e.g. 4-5), without introducing a great issue since these only depend on the knowledge of the initial date and the time step. For this purpose, the chief absolute elements and the angles describing the Earth's position around the Sun are updated, thereby influencing the expressions of the empirical parameters in Equation (12). This adjustment can be appreciated in Figure 2 where the yearly relative eccentricity circulation described is recovered with the same accuracy by the proposed analytical model with empirical parameters updated at each time step, with the benefit of using a very simple STM formulation. Note that, also Spiridonova[10] and Luo *et al.*[9] models employ osculating elements and are not capable of forecasting the periodic effect of the Earth's orbit around the Sun over longer time horizons if the employed parameters are not updated during the simulation.

3.2 Modelling performance: numerical validation

A high fidelity numerical propagation employing the 5th order DOPRI5[3] integrator of Matlab/Simulink® is used to validate the ROEs' evolution computed from the numerically propagated absolute orbits of the two satellites. First, the only perturbation included in the reference is SRP to verify the accuracy of the analytical formulation and how it aligns with the perturbation behaviour as computed from the absolute elements. Subsequently the orbits subject to all perturbations present in the GEO region are used to assess how the SRP model behaves in this realistic scenario, thereby verifying the assumptions made in the model's derivation, starting from the fact that the differential SRP is indeed dominant compared to other perturbations. The validation scenario is described in Table 2.

Chief Initial Keplerian Elements					
$a[km]$	$e[-]$	$i[^\circ]$	$\Omega[^\circ]$	$\omega[^\circ]$	$M[^\circ]$
$4.2164 \cdot 10^4$	0.005	3	60	45	1
Initial Relative Orbital Elements					
$a\delta a[m]$	$a\delta\lambda[m]$	$a\delta e_x[m]$	$a\delta e_y[m]$	$a\delta i_x[m]$	$a\delta i_y[m]$
0	-500	300	300	-300	-300
Mission Timing and Propagation					
Initial Date: 2002-01-01 00:00:00			**Propagation Duration (orbits):** 10		
Propagation Steps Size: $60s$					
SRP Properties					
Chief			**Deputy**		
Area [m^2]	Mass [kg]	c_r	Area [m^2]	Mass [kg]	c_r
4	1000	1.88	1	100	1.88

Table 2: Mission parameters to validate the empirical SRP model, as taken from Guffanti and D'Amico.[8]

Section 3.2 reports the maximum absolute error along the propagation horizon in these two scenarios. The ROEs of the reference integrator are built from the absolute propagation of the orbit of the two spacecraft, and the error is also due to the variation of these parameters along the integration. To cope with this situation, these were updated at each time step and fed to the model, similarly to what would realistically happen with the onboard navigation being updated with data from the ground regarding the absolute behaviour of the target. Moreover, two different pre-processing of the chief absolute elements were considered before feeding them to the empirical coefficients computations: these were either directly used or, in the other case, averaged on a 1 orbit window.

DOI: 10.13009/EUCASS2025-325

SRP Only						
HCW	64.5979	193.1709	2.7788	0.0043	0.0089	$2.8188 \cdot 10^{-4}$
ROE	1.2627	70.4158	20.3967	20.8384	1.3939	1.2169
True						
HCW	63.8719	182.4813	3.4364	0.0042	0.0088	$3.1009 \cdot 10^{-4}$
ROE	1.2695	61.8935	19.4258	20.2509	3.0672	0.9907

Table 3: Maximum absolute error along the 10 orbit validation. HCW errors are measured in [m] and [m/s], while dimensional ROEs are measured in [m].

An important improvement from updating the empirical parameters is the capability to describe the long-term effects. The most important one in the case of SRP is the yearly circulation of the relative eccentricity vector.[8] The adherence of the model to this effect is shown in Figure 2.

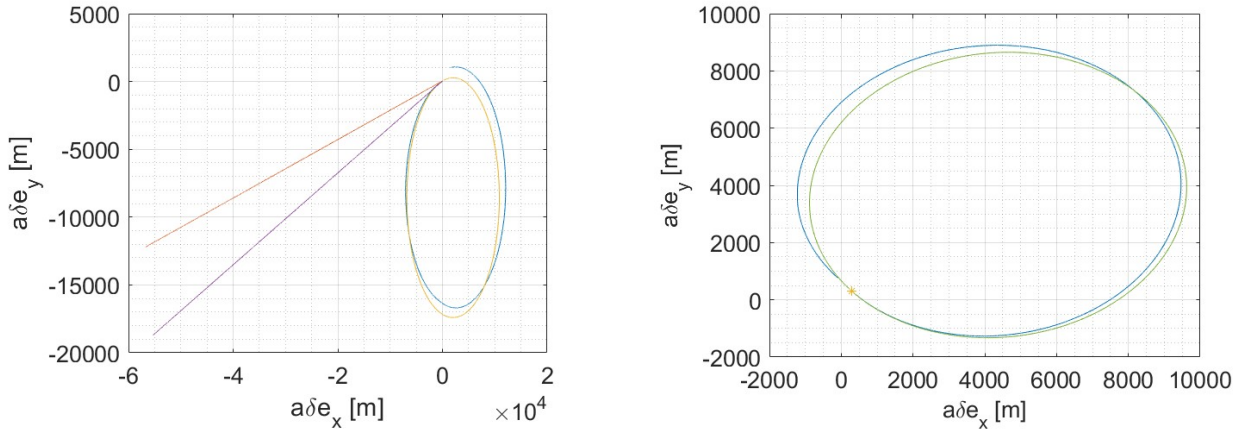

Figure 2: Yearly relative eccentricity circulation in the literature comparison and in the numerical validation. The blue line represents the empirical formulation, while the models from the literature are shown in orange ([9]), purple ([10]), and yellow ([8]). The green line refers to the DOPRI5 integrator results.

4. Use of the model

This section exploits the analytical model and leverages the ROE geometrical understanding of the perturbed motion to assess how the relative trajectory evolves under the effect of differential SRP, starting at different times and dates. This knowledge is the foundation of passive safety concepts, which are adapted from the E/I separation and specific for the GEO scenario, both for bounded and high-drift motion. A case scenario far-range RV that exploits impulsive manoeuvre schemes from the literature is designed, implementing the newly developed safety concepts and comparing different alternatives in terms of safety and fuel expenditure.

4.1 Analyses of the departure time of close-range rendezvous

The evolution of the ROE state at different times of the day Figure 3 is analysed to advance the discussions in Fehse[4] carried out in the HCW framework.

- The relative semi-major axis oscillates with an amplitude $a\delta a_{\text{amplitude}} = \frac{2}{n^2}\sqrt{A_R^2 + B_R^2}$ and with a mean value $a\delta a_0 = -\frac{2}{n^2}A_{R,0}$. For $|a\delta a_0| >> 0$ the natural motion rules on the perturbed effect, while for $|a\delta a_0| \approx 0$ the direction can reverse depending on the departure time;
- The V-bar motion is influenced in terms of $a\delta\lambda$ by means of the Keplerian coupling $-\frac{3}{2}nta\delta a_0$;
- The evolution of the relative eccentricity vector looks linear in the short term (e.g. 5-10 orbits). The constant slope in the $a\delta e_x/a\delta e_y$ plane is $\phi_{\text{linear}} = \arctan\frac{a\delta\dot{e}_y}{a\delta\dot{e}_x}$. In the long term, a yearly circulation takes place.[8] The starting phase on the $a\delta e_x/a\delta e_y$ circumference depends on the initial time;

DOI: 10.13009/EUCASS2025-325

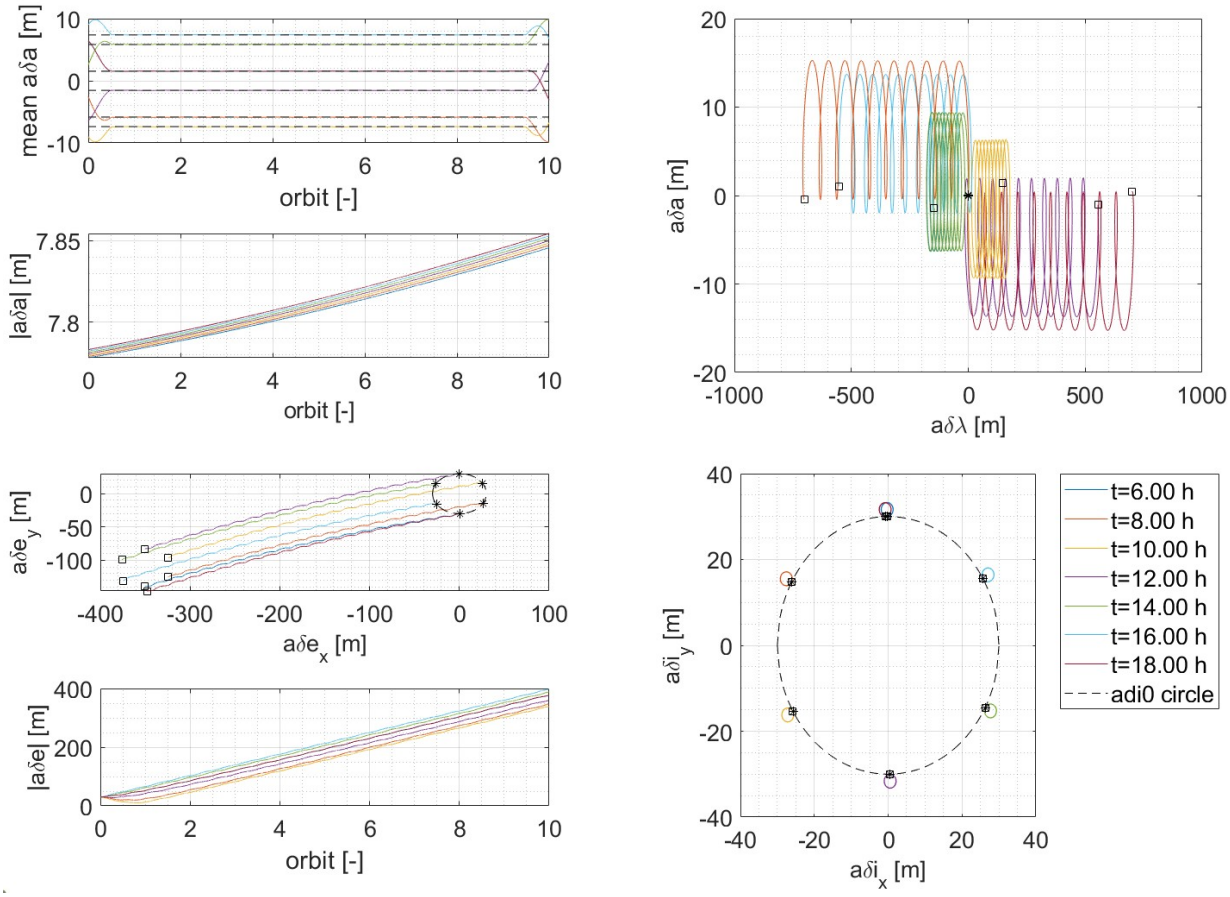

Figure 3: Respectively $a\delta a$ properties, $a\delta \boldsymbol{e}$ plane and magnitude, $a\delta\lambda/a\delta a$ plane, and $a\delta \boldsymbol{i}$ plane at different departure times

- The relative inclination vector shows a circular motion of radius $a\delta i_{\text{radius}} = z_{\text{oop}}$, with initial phase and centre position depending on the time of interrupted station keeping, similarly to what happens to $a\delta \boldsymbol{e}$.

4.2 Enhance passive safety design accounting for SRP

Passive safety refers to the property of a relative trajectory to remain collision-free for a given time duration with no control action. This aspect is of extreme criticality in the context of proximity operations in OOS missions, to avoid collisions with the uncooperative target in case of actuator failures. The E/I separation concept, initially developed for GEO satellites collocation, is broadly used and is based on the fact that the navigation estimation error in the along-track direction is, in general, much larger than the radial and cross-track component.[2] Given the presence of SRP, the safety of the configuration in perturbed motion depends on the time of the year, which influences the $a\delta \boldsymbol{e}$ slope. Two concepts are developed here to support two different phases of the RV:

- **Bounded motion:** The relative perigee ϕ shall be selected as $\phi_{\text{start}} = \phi_{\text{linear}}$, with ϕ_{linear} being the constant slope in the relative eccentricity plane under the effect of differential SRP, and a (anti-) parallel phasing of the relative ascending node. For values $\phi_{\text{start}} \in \{\phi_{\text{linear}} \pm \frac{\pi}{2}\}$, the phasing is retained for a shorter time, but the minimum $a\delta e_0$ value is not violated in this range. Referring to the left figure in Figure 4, the safe region is the green cone. Since the relative inclination magnitude doesn't vary significantly, the increasing magnitude of the relative eccentricity ensures that the minimum RN distance is not violated.
- **High-drift:** The main concern is here to avoid the uncontrolled motion to intersect the along-track in case of a missed burn, and, additionally, to remain confined in a bounded cylinder to reduce the risk

DOI: 10.13009/EUCASS2025-325

of impact with other spacecraft in the region. When the relative eccentricity vector evolves inside the circumference of radius $|a\delta e_0|$, the RN motion will be confined within this value, and thus by selecting $\phi_{\text{drift}} = \phi_{\text{linear}} + \pi$ this confining effect is exploited for the longest time (the whole diameter is covered). The value of $a\delta e_0 = |-\frac{3}{2n}\frac{\Delta t_{\text{drift}} B_R}{2\cos\phi_{\text{linear}}}|$ can be selected exploiting Equation (14) as long as the linear approximation is valid to ensure the confined motion along the drift. The right plot in Figure 4 shows how the blue curly line, which is the perturbed motion in the relative eccentricity plane, remains confined in the initial circle of magnitude $a\delta e_0$ when the concept is applied. The relative phasing angle (defined as $\psi = \phi - \theta$) shall be selected as $\psi = \pm\pi/2$ to further reduce the collision risk during the drift. However, this adjustment can be neglected due to the large radial separation, resulting in a lower fuel expenditure. Indeed, a critical phase in the RV is the transition between high drift to bounded motion, when the radial separation is reduced (braking phase). Here, a relative inclination vector with larger magnitude would finally guarantee greater RN minimum distance for a configuration that exploits these guidelines.

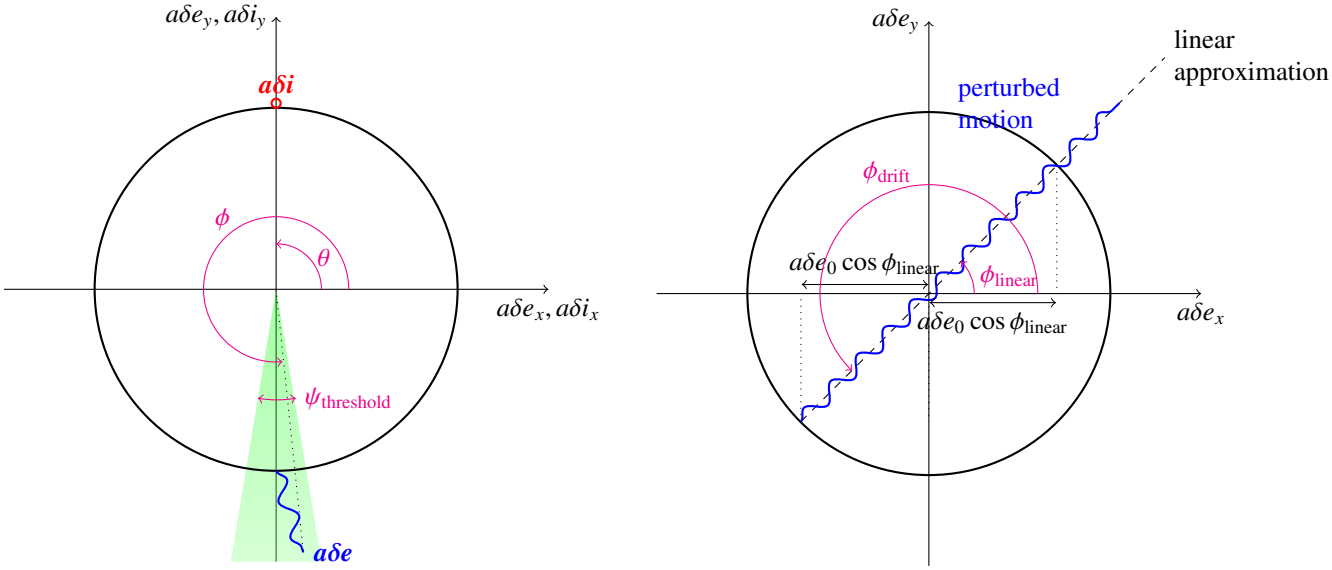

Figure 4: Passively safe phasing of $a\delta\boldsymbol{e}/a\delta\boldsymbol{i}$ for bounded and high-drift motion.

The bounded passive safety concept is assessed for different times of the year, exploiting as a figure of merit the phasing of the $a\delta\mathbf{e}/a\delta\mathbf{i}$ vectors (initially anti-parallel) and the one-orbit minimum distance in the RN plane, computed with the procedure of the Onboard Safety Monitoring (OSM) from AVANTI[5] (Figure 5).

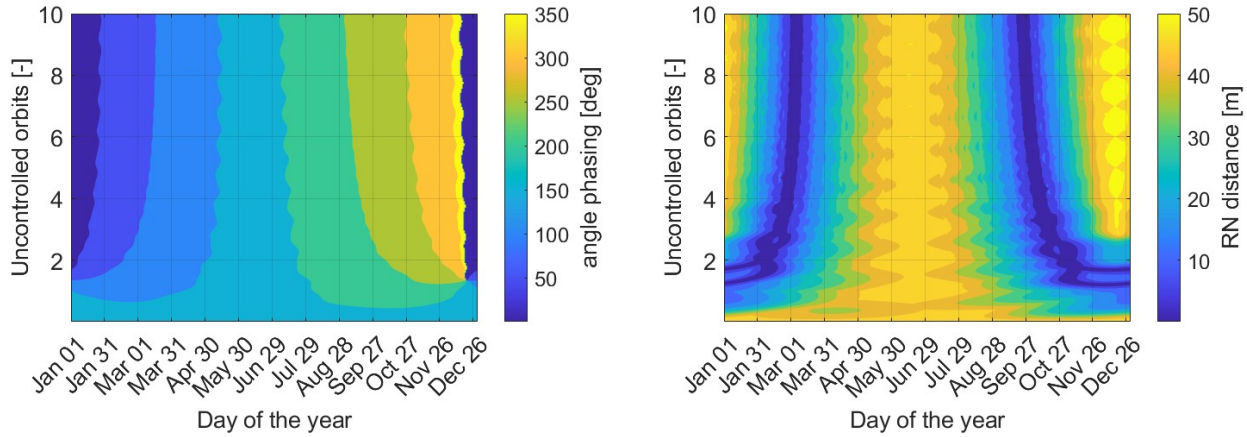

Figure 5: Phasing and RN minimum distance for 100 uncontrolled orbits starting from $a\delta\boldsymbol{\alpha_0} = [0,\ 0,\ 0,\ 50,\ 0,\ -50]m$

For a starting date set as January 1st 2000 at noon, Figure 6 shows the effectiveness of this method in

DOI: 10.13009/EUCASS2025-325

keeping the norm of $a\delta\boldsymbol{e}$ below its initial value, for the given duration of 4 orbits.

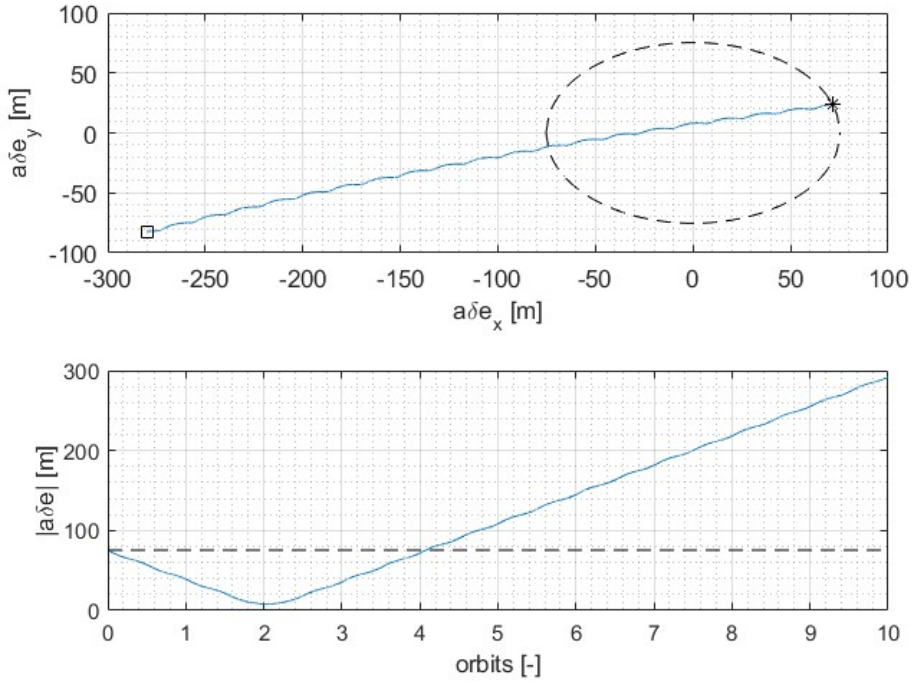

Figure 6: Evolution of $\boldsymbol{a\delta e}$ when applying the concept for safety along the drift. Black dashed lines represent $a\delta e_0$.

4.3 Rendezvous design including SRP modelling and developed safety measures

The SRP empirical model has proved its validity in the design of a case-scenario RV. Fuel-consumption and operational considerations may lead to the introduction of high-drift phases to exploit the natural motion, in order to minimise the fuel consumption. The trajectory is planned by comparing different control schemes and making use of the safety concepts introduced in Section 4.2. The far-range RV is designed here starting from an initial point $a\delta\boldsymbol{\alpha_0}$ at the edge of the co-location slot to a final offset along the V-bar of 500 meters. Table 4 resumes the ballistic coefficient properties, taken as similar to the spacecraft involved in the MEV 1 mission. Section 4.3 resumes the ROE sets computed with these procedures. Figure 7 shows the ideal evolution starting from the desired ROEs at each segment, encompassing the desired safety concept and directly shifting through each ROE set, that is without considering the real manoeuvre errors that come from the differential SRP perturbation between the pulses.

SRP Properties					
Intelsat 901 (Chief)			**MEV 1-2 (Deputy)**		
Area [m^2]	Mass [kg]	c_r	Area [m^2]	Mass [kg]	c_r
60	4723	1.2	20	2326	1.2

Table 4: SRP properties for the RV design.

The control schemes considered from the literature are:

- Control layer scheme from Autonomous Vision Approach Navigation and Target Identification (AVANTI) experiment. It involves 3 in-plane pulses and 1 out-of-plane pulse;
- Bounded relative motion control scheme from GEO re-location. It involves 2 in-plane pulses and 1 out-of-plane pulse;
- manoeuvres to reach/leave the drift segment.

DOI: 10.13009/EUCASS2025-325

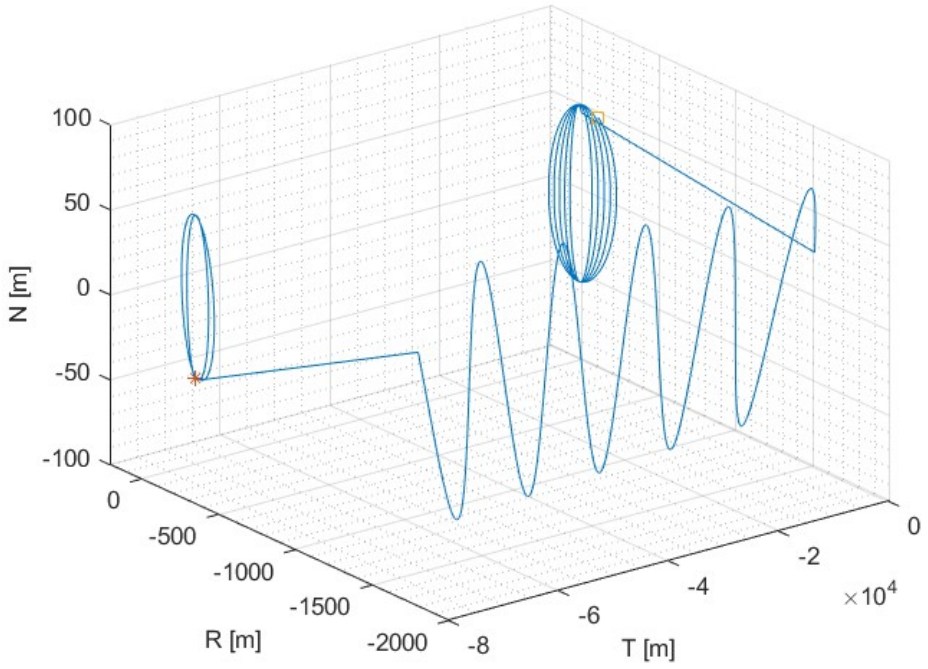

Figure 7: Ideal Cartesian evolution without manoeuvres effect. The star represents the starting point, and the square represents the desired configuration.

Reconfiguration ROE sets [m]						
Initial	5	-70000	0	50	0	-50
Drift	$-1.4748 \cdot 10^3$	-70000	-26.3865	64.9920	-64.9920	-26.3865
Intermediate brake	-737.4179	-10000	18.8088	-46.3274	18.8088	-46.3274
V-bar intermediate brake	0	-1000	18.8088	-46.3274	18.8088	-46.3274
Final	0	-500	18.8088	-46.3274	18.8088	-46.3274

Table 5: Intermediate ROE sets across the reconfiguration

Such control schemes have been included in the following guidance strategies:

- **RV1**: A single 3T-1N scheme;
- **RV2**: 3T-1N scheme to reach/leave the drift segment (with or without intermediate brake).
- **RV3**: Tangential burns to reach and leave the drift segment, and 3T-1N scheme achieve the end conditions;
- **RV4**: Tangential burns to reach and leave the drift segment, and scheme for GEO re-location at the end;

Particular attention is paid to the transition between high-drift and bounded motion since it encompasses a change of the safety concept when the along-track with the target has already been reduced.

Figure 8 shows the evolution of the RN minimum distance for the described guidance profiles, while Figure 9 represents the pulse magnitudes along the RV.

The braking phase is critical: a transition between the high-drift and bounded passive safety concept must take place, and the radial distance is reduced when the along-track separation has already been removed. For this reason, an additional guidance profile that divides this phase into two parts, reaching the intermediate configuration with an application of the 3T-1N scheme, is also analysed. This method shows to effectively increase the safety of the RV, and the minimum RN distance and pulse magnitude in this case are reported in Figure 10.

Table 6 resumes the fuel consumption and the overall duration of the various reconfiguration methods.

Some considerations regarding the different strategies are the following:

DOI: 10.13009/EUCASS2025-325

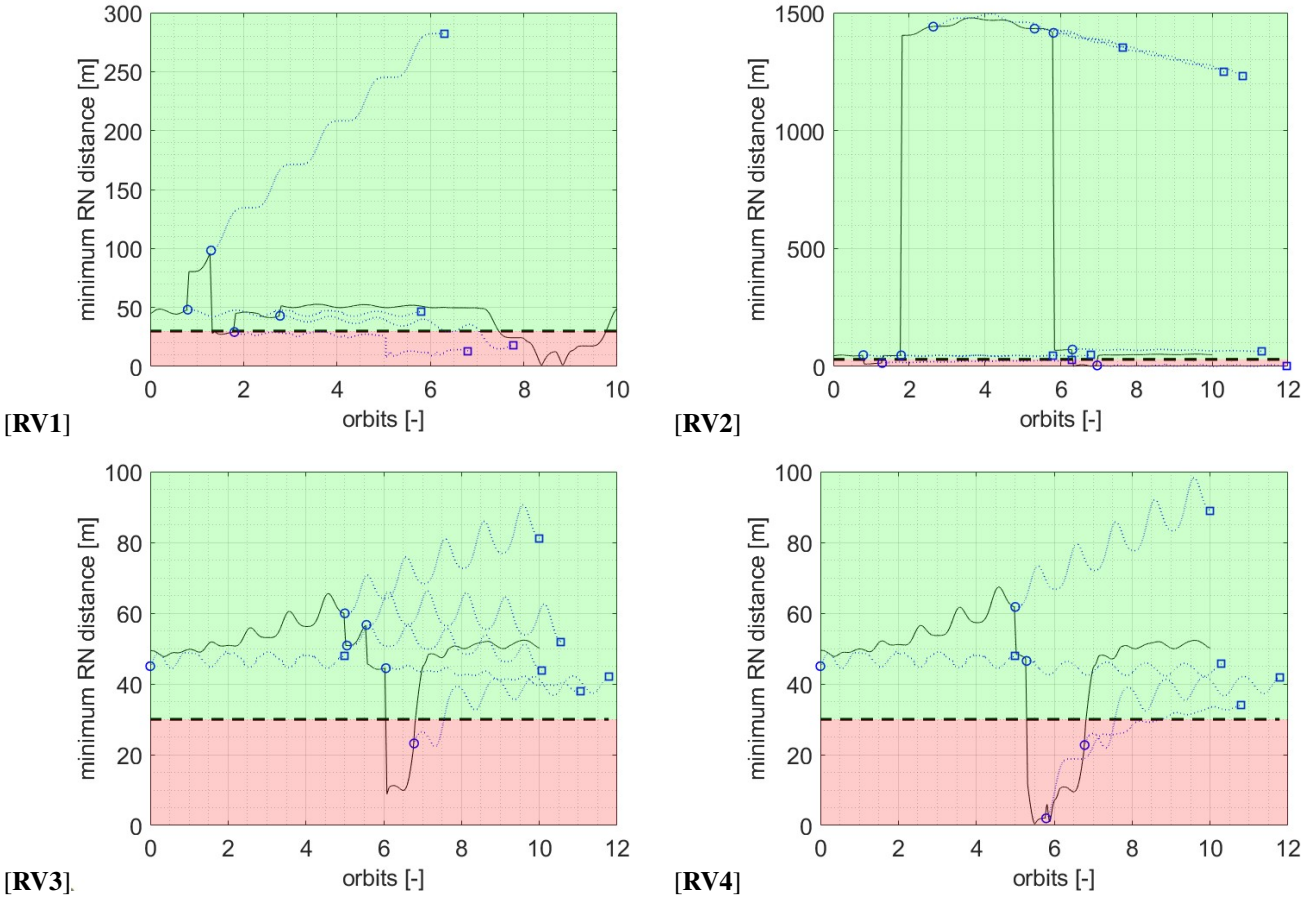

Figure 8: Minimum RN distance evolution: the uncontrolled motion - stemming from the last executed manoeuvre - is computed for 10 orbits. The green region characterises passively safe trajectories, the red one indicates a violation of the minimum 30 m threshold.

Control Scheme	Fuel Consumption [m/s]	Reconfiguration Time [days]	Total Pulses
RV1	0.5467	2.7732	4
RV2	0.2648	6.9444	8
RV3	0.1135	6.7623	6
RV4	0.1234	6.7623	5
RV2 with intermediate brake	0.1820	9.5324	12

Table 6: Performance metrics for various control schemes.

- The application of the 3T-1N scheme once, although providing the shorter time of reconfiguration, also needs the higher fuel expenditure and does not take into account the passive safety concept for the transition between bounded and high drift phases, thus resulting in unsafe trajectories, particularly in the last part of the RV, the most critical.
- The strategies involving simple tangential burns to enter and leave the high drift provide the lower bound for fuel usage, but result in a poorly safe brake phase initially (the second T pulse cannot ensure proper phasing of the relative eccentricity), which is then recovered with the final correction manoeuvre. The bounded GEO re-location scheme can guarantee a lower accuracy on the final along-track separation.
- The adoption of the 3T-1N scheme to reach and leave the high drift provides a good trade-off between fuel expenditure and safety, costing far less than the single application of the scheme since the natural drift is exploited to cover the larger separation component, but also ensuring a better capability to

DOI: 10.13009/EUCASS2025-325

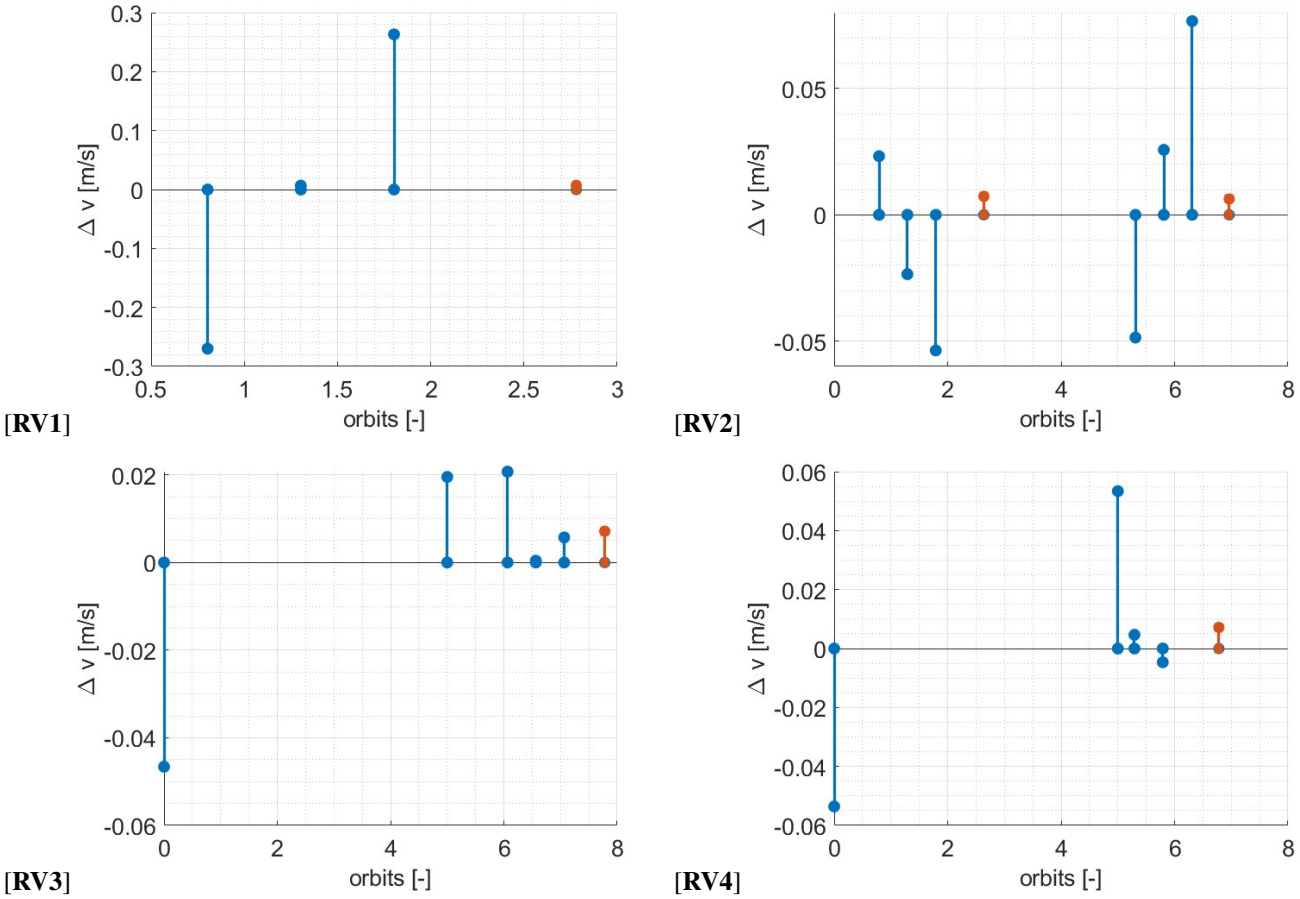

Figure 9: Pulses location and magnitudes. Blue lines represent tangential manoeuvres. Red lines represent normal burns.

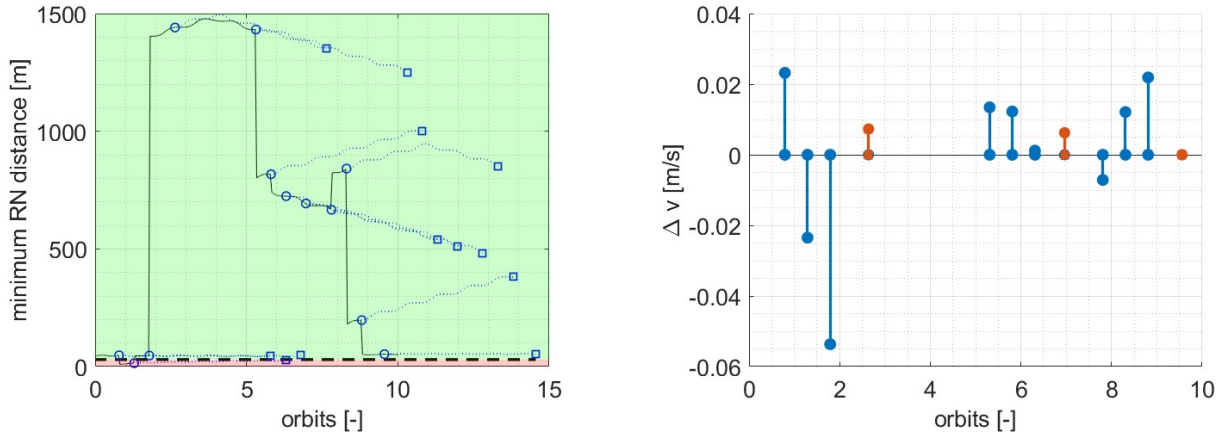

Figure 10: RN distance and pulse magnitude for the best compromise.

control the relative eccentricity and inclination phasing to adhere to the developed guidelines for perturbed passive safety in the GEO scenario. However, this comes at the cost of longer duration of the RV.

- The strategy involving an intermediate brake before reaching the final configuration preserves the passive safety for most of the cases, but results in a longer time of reconfiguration, which may be too extended for the GEO co-location constraints.

DOI: 10.13009/EUCASS2025-325

5. Conclusions

This research aims to develop an empirical model for SRP, which is the most significant differential perturbation in GEO, a region of particular importance for OOS missions. One of the key advantages of this procedure is simplicity, which exploits the natural behaviour of the HCW dynamics to only retain the relevant shape of the input. Starting from the perturbed general solution, any non-gravitational input can be modelled by setting the proper coefficients. The comparison with literature models shows how similar results with respect to case-tailored techniques can be obtained. The numerical validation contributed to assessing the accuracy of the model with respect to more realistic data, proving the validity of the hypothesis of only considering differential SRP as the most relevant perturbation in relative motion in GEO. The ROE framework geometrical insight is successfully exploited to clarify the dependence on the starting time of the RV, overcoming the difficulties found in the HCW framework.

In the context of a far range RV, the developed model is used to tailor an improved version of the E/I safety concept, both for bounded and unbounded phases in SRP highly perturbed environments. The modelled perturbation captures with enough detail the geometrical variations of the formation to design a proper guidance plan. The real implementation using finite burn control schemes may hinder the accuracy of the configuration, thus affecting the ideal safety concepts. Closed-loop control may be required to overcome this issue.

Further refinements can be made by incorporating additional empirical parameters, such as those accounting for other perturbations or combined effects. Eclipses, which are not significant in GEO but could affect other orbital regimes, may be easily modelled by properly updating the empirical coefficients. Although these refinements would improve the model's accuracy, the current formulation remains a practical solution for most OOS missions, offering a good balance between simplicity and effectiveness.

Finally, the use of analytical models, like the one developed here, plays a crucial role in the ongoing shift towards increased satellite autonomy. By reducing the reliance on computationally expensive methods, analytical models help ensure that onboard systems can operate efficiently, supporting mission success with minimal ground intervention.

References

[1] Oscar L Colombo. The dynamics of global positioning system orbits and the determination of precise ephemerides. *Journal of Geophysical Research: Solid Earth*, 94(B7):9167–9182, 1989.

[2] Simone D'Amico and Oliver Montenbruck. Proximity operations of formation-flying spacecraft using an eccentricity/inclination vector separation. *Journal of Guidance, Control, and Dynamics*, 29(3):554–563, 2006.

[3] John R Dormand and Peter J Prince. A family of embedded runge-kutta formulae. *Journal of computational and applied mathematics*, 6(1):19–26, 1980.

[4] W Fehse. Disturbance by solar pressure of rendezvous trajectories in geo, 5th icatt. In *International Conference on Astrodynamics Tools and Techniques, Noordwijk, The Netherlands*, 2012.

[5] Gabriella Gaias and Jean-Sébastien Ardaens. Design challenges and safety concept for the avanti experiment. *Acta Astronautica*, 123:409–419, 2016.

[6] Gabriella Gaias, Jean-Sébastien Ardaens, and Oliver Montenbruck. Model of J2 perturbed satellite relative motion with time-varying differential drag. *Celestial Mechanics and Dynamical Astronomy*, 123(4):411–433, 2015.

[7] Gabriella Gaias and Marco Lovera. Trajectory design for proximity operations: The relative orbital elementsâ perspective. *Journal of Guidance, Control, and Dynamics*, 44(12):2294–2302, 2021.

[8] Tommaso Guffanti and Simone D'Amico. Linear models for spacecraft relative motion perturbed by solar radiation pressure. *Journal of Guidance, Control, and Dynamics*, 42(9):1962–1981, 2019.

[9] Ya-Zhong Luo, Zhen-Jiang Sun, and Jin Zhang. Proximity scenario design for geostationary rendezvous with collocated satellite avoidance. *Acta astronautica*, 154:153–168, 2019.

[10] Sofya Spiridonova. Formation dynamics in geostationary ring. *Celestial Mechanics and Dynamical Astronomy*, 125(4):485–500, 2016.